Parametric amplification in lossy nonlinear waveguides with spatially dependent coupling

VITOR RIBEIRO AND AURO M. PEREGO[*]

Aston Institute of Photonic Technologies, Aston University, Birmingham, B4 7ET, United Kingdom
[*]*a.perego1@aston.ac.uk*

Abstract: We present an analytical and numerical study of optical parametric amplification in coupled waveguides amplifiers accounting for presence of losses and spatially dependent coupling. Spatially dependent coupling enables to compensate for mismatch dynamically arising from pump attenuation and to achieve improved performances in terms of bandwidth and bandwidth-gain product compared to standard single-waveguide solutions. Our results suggest the effective design of a novel class of parametric amplifiers and could be especially relevant for integrated silicon nitride devices.

1. Introduction

The constantly growing demand for increasing information data rate transmitted in optical communications, required by the pivotal role played by internet in modern interconnected societies, is driving research towards solutions capable of expanding the spectral bandwidth (BW) of transmitted signals. Broadband signal spectrum requires equivalently broadband amplifiers to regenerate signals upon propagation along optical fiber systems. Currently the workhorse for signal amplification in commercially available fiber optics communication systems are Erbium-doped fiber amplifiers (EDFAs) [1,2] which cover a BW of approximately 40 nm.

However alternative broad band solutions such as Raman fiber amplifiers [3], semiconductor optical amplifiers [4] and optical parametric amplifiers [5–8] are currently being actively investigated. In particular, optical parametric amplifiers are excellent candidates for broadband amplification exceeding 100 nm [9]. Parametric amplifiers operate based the on the physical phenomenon of modulation instability [10,11] originally demonstrated in single mode fibers more than 30 years ago [12]. Modulation instability refers to energy transfer from a powerful pump wave to symmetrically located spectral sidebands (called Stokes and anti-Stokes waves) thanks to the interplay between cubic Kerr nonlinearity and anomalous group velocity dispersion. This is more generally described within the so called four-wave mixing process where, provided certain phase-matching conditions associated to energy and momentum conservation are satisfied, two photons from the pump frequency are annihilated and one photon at signal and idler frequency respectively are created [13].

Not relying on stimulated emission process parametric amplifiers are immune to quantum noise added to the signal upon interaction with the gain medium, and their noise properties are limited by the input noise of the pump wave potentially reaching a zero dBs noise figure in the phase-sensitive configuration [14–16]. Parametric amplification has been investigated theoretically, experimentally or both, especially in silica fibers platforms, where a variety of architectures have been explored. Among these we mention the possibility of phase sensitive amplification exploiting phase relation between pump signal and idler waves [17], Raman assisted parametric amplification [9], polarisation diverse schemes [18], quasi phase-matching [19,20], dual-core (DC) fibers [21,22], and multimode fibers [23].

Recent advances in silicon nitride waveguides fabrication techniques have enabled the demonstration of parametric amplification in integrated devices too [24]. Besides the potential for ultra small dimensions (a fixed height of 950 nm and different widths ranging from 600 nm

to 1500 nm has been reported in [25]), the absence of Brillouin scattering in silicon nitride eliminates one of the major impairments which affects the operation of silica fibers parametric amplifiers requiring phase-modulation (dithering) of the pump: 20 kW stimulated Brillouin scattering threshold has been demonstrated for 1 m of silicon nitride waveguide [26], which compares to 100 W in silica single mode fiber with the same length. However silicon nitride waveguides suffer from strong losses of the order of 1 dB/m [27], which makes the spatial scale over which pump attenuation takes place comparable to the nonlinear length of the system which is the characteristic scale of the amplifier gain performances. While the theory of modulation instability in presence of frequency independent losses [28] and the expression for the parametric amplifier gain in a lossy fiber [29] have been obtained some years ago, a first theoretical study of the impact of losses in realistic silicon nitride parametric amplifiers has been presented only recently in [30] using an approximation analogous to that of [29] based on the replacement of the amplifier length with the losses effective length. It has been furthermore suggested that waveguide tapering resulting in a spatially decreasing group velocity dispersion could compensate for the losses induced change in the mismatch parameter (leading to a reduction of the nonlinear contribution) hence preventing performance degradation [31]. While two-photon absorption (TPA) can indeed influence processes based on modulation instability phenomena [32], silicon nitride has favourable characteristics for parametric amplification since it is not affected by TPA for wavelengths above 800 nm [33] and therefore supports high pump powers.

In this article we present the theoretical and numerical study of a parametric amplifier consisting of two evanescently coupled waveguides, including the effect of optical losses but especially investigating the role of spatially dependent coupling. Parametric amplification in dual-waveguide (DW) fibers with coupled cylindrical core has been proposed theoretically, promising wide bandwidth, flat broadband gain spectrum, exponential evolution of the gain over the propagation length, [21] and 0 dBs noise figure, when operated in phase-sensitive mode [22]. In [22] the possibility was explored to use the coupling of the two waveguides instead of the customary nonlinear coupling provided by the pump in single-waveguide (SW) parametric amplifiers, in order to provide the necessary interference between the signal and its copy. This allows to achieve a 6 dBs gain advantage over phase-insensitive mode of operation, and it is beneficial since the coupling, not possessing phase, makes the phase-sensitive gain dependent only on the relative phase between signal in the first waveguide and its copy in the second waveguide. In this way it is possible potentially to avoid state of the art solutions using pump recovery [8]. A first attempt to manufacture such DWs using cylindrical core single mode fibers for the purpose of parametric amplification and wavelength conversion was made in [34]. In this work we fully generalise and improve the formalism developed in [21] for a conservative scenario and with constant coupling, making it suitable for realistic applications both in integrated coupled waveguides and in coupled core silica fibers too. Our numerical results, obtained with realistic parameters for silicon nitride waveguides show that the DW architecture with spatial dependent coupling can provide, for certain parameters, a broader gain spectrum and an increased bandwidth-gain (BWG) product compared to a SW device even when fiber tapering is included.

The paper is structured as follows. In section 2 the general analytical theory of parametric amplification in coupled waveguides with spatially dependent coupling and losses is formulated and presented. In section 3 the analytical predictions for the amplifier gain are compared with numerical simulations results. In section 4 a performance comparison with realistic lossy silicon nitride waveguides based parametric amplifiers with and without dispersion management is presented. Conclusions are discussed in section 5.

2. Analytical theory

We consider two identical coupled waveguides where the electric fields slowly varying envelope evolution is described by two coupled nonlinear Schrödinger equations (NLSEs)

$$
\begin{aligned}
\frac{\partial U_1}{\partial z} &= i\sum_{n=2}^{\infty} i^n \frac{\beta_n}{n!}\frac{\partial^n U_1}{\partial t^n} + i\gamma U_1|U_1|^2 - \frac{\alpha}{2}U_1 + iC(z)U_2 \\
\frac{\partial U_2}{\partial z} &= i\sum_{n=2}^{\infty} i^n \frac{\beta_n}{n!}\frac{\partial^n U_2}{\partial t^n} + i\gamma U_2|U_2|^2 - \frac{\alpha}{2}U_2 + iC(z)U_1.
\end{aligned}
\tag{1}
$$

Here $U_{1,2}$ are the two field amplitudes defined in a co-moving temporal reference frame of coordinate t and evolving along spatial coordinate z. γ, β_n and α are nonlinearity, n-th order dispersion and loss coefficient respectively. $C(z)$ denotes the space dependent evanescent coupling strength.

The theory of modulation instability in coupled nonlinear waveguides has been developed for a series of particular cases [35–43], but only recently a first description of a parametric amplifier based on coupled waveguides (specifically dual coupled core single-mode fibers) has been developed obtaining an analytical solution [21,22].

Starting from Eq. (1) it is possible to derive the coupled evolution equations for the pump (u_{p1}, u_{p2}), signal (u_{s1}, u_{s2}), and idler (u_{i1}, u_{i2}) wave amplitudes, where the subscripts $1, 2$ refer to the two waveguides respectively and the subscripts p, s, i refer to quantities connected to pump, signal and idler waves:

$$
\begin{aligned}
\frac{\partial u_{p1}}{\partial z} &= iu_{p1}\left(\beta_{p1} + \gamma(2P_1 - |u_{p1}|^2)\right) + i\gamma 2u_{p1}^* u_{s1}u_{i1} + iC(z)u_{p2} - \frac{\alpha}{2}u_{p1} \\
\frac{\partial u_{s1}}{\partial z} &= iu_{s1}\left(\beta_{s1} + \gamma(2P_1 - |u_{s1}|^2)\right) + i\gamma u_{p1}^2 u_{i1}^* + iC(z)u_{s2} - \frac{\alpha}{2}u_{s1} \\
\frac{\partial u_{i1}}{\partial z} &= iu_{i1}\left(\beta_{i1} + \gamma(2P_1 - |u_{i1}|^2)\right) + i\gamma u_{p1}^2 u_{s1}^* + iC(z)u_{i2} - \frac{\alpha}{2}u_{i1} \\
\frac{\partial u_{p2}}{\partial z} &= iu_{p2}\left(\beta_{p2} + \gamma(2P_2 - |u_{p2}|^2)\right) + i\gamma 2u_{p2}^* u_{s2}u_{i2} + iC(z)u_{p1} - \frac{\alpha}{2}u_{p2} \\
\frac{\partial u_{s2}}{\partial z} &= iu_{s2}\left(\beta_{s2} + \gamma(2P_2 - |u_{s2}|^2)\right) + i\gamma u_{p2}^2 u_{i2}^* + iC(z)u_{s1} - \frac{\alpha}{2}u_{s2} \\
\frac{\partial u_{i2}}{\partial z} &= iu_{i2}\left(\beta_{i2} + \gamma(2P_2 - |u_{i2}|^2)\right) + i\gamma u_{p2}^2 u_{s2}^* + iC(z)u_{i1} - \frac{\alpha}{2}u_{i2}.
\end{aligned}
\tag{2}
$$

Here $P_1 = |u_{p1}|^2 + |u_{s1}|^2 + |u_{i1}|^2$, $P_2 = |u_{p2}|^2 + |u_{s2}|^2 + |u_{i2}|^2$ and the β coefficients describe the propagation constants. We assume that being the two waveguides identical: $\beta_{p1} = \beta_{p2}$, $\beta_{s1} = \beta_{s2}$, and $\beta_{i1} = \beta_{i2}$.

We now assume that both waveguides are pumped with the same input pump power such that $P_{p1} + P_{p2} = P_p$ and consider the small sidebands approximation, $P_p/2 >> |u_{s,i}|^2$, corresponding to the fact that signals and idlers do not deplete the pump waves. Under this approximation the pump amplitudes admit the following solutions

$$
\begin{aligned}
u_{p1}(z) &= \sqrt{\frac{P_p}{2}}e^{i\phi_0 + i\beta_p z + i\frac{\gamma}{2}\int_0^z P_p e^{-\alpha z'}dz' + i\int_0^z C(z')dz' - \frac{\alpha}{2}z} \\
u_{p2}(z) &= \sqrt{\frac{P_p}{2}}e^{i\phi_0 + i\beta_p z + i\frac{\gamma}{2}\int_0^z P_p e^{-\alpha z'}dz' + i\int_0^z C(z')dz' - \frac{\alpha}{2}z}
\end{aligned}
\tag{3}
$$

where ϕ_0 is a common phase factor. We furthermore write the sidebands amplitudes in the two waveguides as a function of the new amplitudes $e_{s1}(z), e_{i1}(z), e_{s2}(z), e_{i2}(z)$:

$$
u_{s1,i1,s2,i2}(z) = e_{s1,i1,s2,i2}(z)e^{i\phi_0 + i\beta_{s1,i1,s2,i2}z + i\frac{\gamma}{2}\int_0^z P_p e^{-\alpha z'}dz' - i\frac{\Delta\beta}{2}z + i\int_0^z C(z')dz'}
\tag{4}
$$

where $\Delta\beta = \beta_s + \beta_i - 2\beta_p$ is the linear mismatch. Using the above mentioned approximations and definitions we can write the set of linear coupled differential equations ruling the evolution

of $\vec{E} = col(e_{s1}, e_{i1}^*, e_{s2}, e_{i2}^*)(z)$ in matrix form as:

$$\frac{\partial \vec{E}}{\partial z} = M(z)\vec{E} \tag{5}$$

where

$$M(z) = \begin{pmatrix} iK_0(z) - \frac{\alpha}{2} & i\gamma\frac{P_p}{2}e^{-\alpha z} & iC(z) & 0 \\ -i\gamma\frac{P_p}{2}e^{-\alpha z} & -iK_0(z) - \frac{\alpha}{2} & 0 & -iC(z) \\ iC(z) & 0 & iK_0(z) - \frac{\alpha}{2} & i\gamma\frac{P_p}{2}e^{-\alpha z} \\ 0 & -iC(z) & -i\gamma\frac{P_p}{2}e^{-\alpha z} & -iK_0(z) - \frac{\alpha}{2} \end{pmatrix}. \tag{6}$$

$K_0(z) = \gamma\frac{P_p}{2}e^{-\alpha z} + \frac{\Delta\beta}{2} - C(z)$ is the total mismatch parameter accounting for nonlinear, linear and coupling contribution. We can appreciate how losses make the nonlinear contribution spatially dependent. Regarding the linear mismatch, in this study we will consider the presence of the second order dispersion β_2 only, such that $\Delta\beta = \beta_2(\omega_s - \omega_p)^2$ where ω_p and ω_s are the pump and signal frequency respectively; but we emphasize that higher order dispersion can be accounted for by this formalism too.

Equation (5) admits the following approximated analytical solution: $\vec{E}(z) = e^{\int_0^z M(z')dz'}\vec{E}(0) = N(z)\vec{E}(0)$. We start from computing the integral of the matrix M which reads:

$$I(z) = \int_0^z M(z')dz' = \begin{pmatrix} i\overline{K}_0(z) - \frac{\alpha}{2}z & i\gamma\frac{P_p}{2}L_{eff} & iC_{eff} & 0 \\ -i\gamma\frac{P_p}{2}L_{eff} & -i\overline{K}_0(z) - \frac{\alpha}{2}z & 0 & -iC_{eff} \\ iC_{eff} & 0 & i\overline{K}_0(z) - \frac{\alpha}{2}z & i\gamma\frac{P_p}{2}L_{eff} \\ 0 & -iC_{eff} & -i\gamma\frac{P_p}{2}L_{eff} & -i\overline{K}_0(z) - \frac{\alpha}{2}z \end{pmatrix} \tag{7}$$

where $\overline{K}_0(z) = \gamma\frac{P_p}{2}L_{eff} + \frac{\Delta\beta}{2}z - C_{eff}$ and we have defined a losses effective length $L_{eff} = \frac{1-e^{-\alpha z}}{\alpha}$, and the effective coupling $C_{eff} = \int_0^z C(z')dz'$.

Knowing $I(z)$ we can now proceed to calculate the matrix exponential $e^{I(z)}$. This results in a very large matrix of the form

$$N(z) = e^{I(z)} = \begin{pmatrix} A & B & C & D \\ B^* & A^* & D^* & C^* \\ C & D & A & B \\ D^* & C^* & B^* & A^* \end{pmatrix}. \tag{8}$$

The matrix elements are:

$$\begin{aligned} A &= \frac{1}{2}e^{-\frac{\alpha}{2}z}\left(\cosh\left(\sqrt{\sigma}\right) + \frac{\sqrt{\rho}\cosh(\sqrt{\rho})+i\theta\sinh(\sqrt{\rho})}{\sqrt{\rho}} + \frac{i\chi\sinh\left(\sqrt{\sigma}\right)}{\sqrt{\sigma}}\right) \\ B &= i\frac{1}{4}e^{-\frac{\alpha}{2}z}\gamma P_p L_{eff}\left(\frac{\sinh(\sqrt{\rho})}{\sqrt{\rho}} + \frac{\sinh(\sqrt{\sigma})}{\sqrt{\sigma}}\right) \\ C &= \frac{1}{2}e^{-\frac{\alpha}{2}z}\left(\cosh\left(\sqrt{\sigma}\right) - \cosh\left(\sqrt{\rho}\right) + \frac{i\chi\sinh\left(\sqrt{\sigma}\right)}{\sqrt{\sigma}} - i\frac{\theta\sinh(\sqrt{\rho})}{\sqrt{\rho}}\right) \\ D &= i\frac{1}{4}e^{-\frac{\alpha}{2}z}\gamma P_p L_{eff}\left(\frac{\sinh(\sqrt{\sigma})}{\sqrt{\sigma}} - \frac{\sinh(\sqrt{\rho})}{\sqrt{\rho}}\right); \end{aligned} \tag{9}$$

where

$$\begin{aligned} \sigma &= -\left(\gamma P_p L_{eff} + \frac{\Delta\beta}{2}z\right)\frac{\Delta\beta z}{2}, \quad \rho = \left(2C_{eff} - \frac{\Delta\beta}{2}z\right)\left(-2C_{eff} + \gamma P_p L_{eff} + \frac{\Delta\beta}{2}z\right), \\ \theta &= \left(-2C_{eff} + \frac{\gamma P_p L_{eff}}{2} + \frac{\Delta\beta}{2}z\right), \quad \chi = \left(\frac{\gamma P_p L_{eff}}{2} + \frac{\Delta\beta}{2}z\right). \end{aligned} \tag{10}$$

Given the initial conditions $\vec{E}(0) = col(e_{s1}, e_{i1}^*, e_{s2}, e_{i2}^*)(0)$ one can compute the evolution of signals and idlers amplitudes after propagation distance L by multiplying the initial condition vector by the matrix $N(z)$ evaluated at $z = L$. These solutions enable to calculate the amplifier gain for arbitrary initial conditions and both in the phase-sensitive and phase-insensitive operational regime.

3. Numerical-analytical comparison

We have performed numerical simulations using $\vec{E}(0) = col(e_{s1}(0), 0, e_{s2}(0), 0)$, with $e_{s2}(0) = -e_{s1}(0)$ as initial conditions. The input signal is a comb of continuous waves (CWs) equally spaced by 0.8 nm, and each with -70 dBm power, in order to avoid pump depletion and additional nonlinear crosstalk terms that could eventually interfere with gain computation. The pump power per waveguide considered was 3 W (total power, $P_p = 6$ W), the pump wavelength $\lambda_p = 1560$ nm, $\gamma = 1.2$ W^{-1}m^{-1}, the loss coefficient $\alpha = 3$ dB/m, $L = 6$ m is the length of the waveguide. Different values of β_2 have been considered in our study, including spatially dependent scenarios as well; and are specified later. These parameters are the DW equivalent to those considered in [30]. The coupling coefficient has been taken with the following functional form $C(z) = C(0)e^{-c\alpha z}$, which is set in order to have the best properties of phase matching and gain flatness over a wide-bandwidth which corresponds to low values of the mismatch parameter $K_0(z)$; $C(0) = \frac{\gamma P_p}{4}$ is the coupling coefficient at the waveguide input, i.e. at $z = 0$. The aforementioned functional form makes the two waveguides getting further apart towards the amplifier end at a rate proportional to parameter c and to the loss coefficient of the waveguide α.

This is schematically shown in Fig. 1, where we present the simulation setup for the coupled waveguide system, where the two waveguides get further apart along the silicon nitride amplifier following an exponential decreasing evolution of the coupling.

The simulation setup consists of a high power CW pump, separated by a designated wavelength shift in nm from the zero dispersion wavelength in order to match the dispersion of the waveguides. Both signal and pump waves are mixed together by a 50/50 coupler and 50% of each wave is reintroduced in each waveguide. With the aid of the phase-shifting provided by the 50/50 coupler and the $\frac{\pi}{2}$ phase-shifting provided by the phase-shifter (PS), at the input of the DWs the pump/signal wave in waveguide 1 is co-phased/counter-phased, with respect to the pump/signal wave in waveguide 2, respectively. This allows to have the nice properties of flat, wide and low noise figure of the amplifier as described in [21,22]. The signals and pump propagate through the silicon nitride DW and after proper phase re-alignment, signal waves exit from one port and pump waves exit from the other port of the output coupler, due to constructive/destructive interferference properties of the 50/50 coupler. An experimental implementation of this setup will require phase-locking the pumps and matching their amplitudes at the input of the DWs, otherwise there will be an exchange of power between the cores upon propagation due to the coupling. The DW amplifier with couplers constitutes basically a Mach-Zehnder interferometer. If the phase-shifts on both arms of the Mach-Zehnder interferometer are identical no pump power will leak into the "Signal out" port. Moreover pump power in "Pump out" port shall be stable (continuous wave), if not we will know that the pump phases and amplitudes at the DW input are different. We can therefore monitor the pump power in the "Pump out" port and compare it with a reference signal in order to create an error signal, which, by using a proportional integrator derivative (PID) controller, will tune the PS at the input of the DW in order to lock the phases of the pumps. In order to monitor the power of the pumps 1% tap couplers can be used. See for example [44] for an experimental demonstration of the phase-locking system.
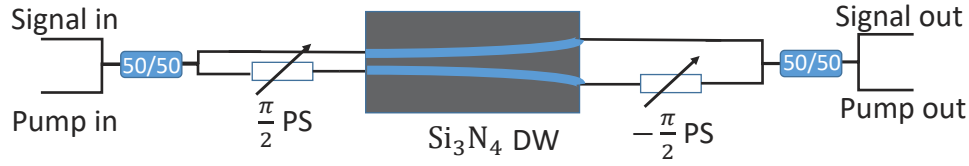
Fig. 1. Setup/schematic of the coupled waveguides amplifier with spatially dependent coupling. PS, phase-shifter.

The gain for the DW amplifier can be computed as

$$G(z) = \frac{\left| \frac{\sqrt{2}}{2} e_{s1}(z) - \frac{\sqrt{2}}{2} e_{s2}(z) \right|^2}{\left| \frac{\sqrt{2}}{2} e_{s1}(0) - \frac{\sqrt{2}}{2} e_{s2}(0) \right|^2} \tag{11}$$

where the $\frac{\sqrt{2}}{2}$ factor is related with the transfer matrix function of the input and output 50/50 couplers [45]. To calculate the gain in the SW case, we set the coupling coefficient $C = 0$ and obtain:

$$G_{SW}(z) = \frac{|e_{s1}(z)|^2}{|e_{s1}(0)|^2}. \tag{12}$$

In order to validate the analytical model described in section 2, we simulated the coupled NLSEs (1) with a split step Fourier transform (SSFT) method. If we set the linear and nonlinear operators as $D_k = i \sum_{n=2}^{\infty} i^n \frac{\beta_n}{n!} \frac{\partial^n}{\partial t^n} - \frac{\alpha}{2}$ and $N_k = i\gamma |U_k|^2$ where k is the waveguide index number, the SSFT method solves Eq. 1) by giving the solution of the DWs at each interval dz, and coupling them by a 2x2 coupler transfer matrix $R(z)$ given by [46]:

$$R(z) = \begin{pmatrix} \cos(C(z)dz) & i\sin(C(z)dz) \\ i\sin(C(z)dz) & \cos(C(z)dz) \end{pmatrix}. \tag{13}$$

Note that $R(z)$ provides the solution of the system neglecting D_k and N_k operators from (1). Therefore at each step dz the solution of Eq. (1) is given by

$$\begin{pmatrix} U_1(z+dz) \\ U_2(z+dz) \end{pmatrix} \approx R(z) \begin{pmatrix} e^{D_1 dz/2} e^{N_1 dz} e^{D_1 dz/2} U_1(z) \\ e^{D_2 dz/2} e^{N_2 dz} e^{D_2 dz/2} U_2(z) \end{pmatrix}. \tag{14}$$

This solution is valid for dz much shorter than the characteristic lengths of the DW system, i e., coupling length, nonlinear length and dispersion length. Figure 2 shows the comparison between analytical solutions developed in section 2 and the SSFT method solution of Eq. (1).

We can see an excellent agreement between theory and numerical simulations for the spatially varying coupling case where $C(z) = C(0)e^{-c\alpha z}$ with $C(0) = 1.8$ m^{-1} and $c = 1$. However in the case of constant coupling, $C(z) = C(0)$, the agreement is good only at small propagation distance and discrepancies arise when $z \geq L_{eff} \approx \frac{1}{\alpha} = 1.42$ m (note that this is analogous to the failure of the theoretical model of a SW lossy parametric amplifier at large distances [30]). From Fig. 2 we can appreciate the superior performances of the spatially varying coupling scenario compared to the constant coupling one. Figure 2(b), 2(c) and 2(d) shows the respective gain spectrum for $z = 1$, $z = 2.4$ and $z = 6$ m. Superior agreement between analytical and the numerical solution of Eq. (1) is achieved for shorter propagation distances and for spatially dependent coupling case. From Figs. 2(b)–2(d) we notice that the numerical solution of Fig. (1) (solid lines), results in an
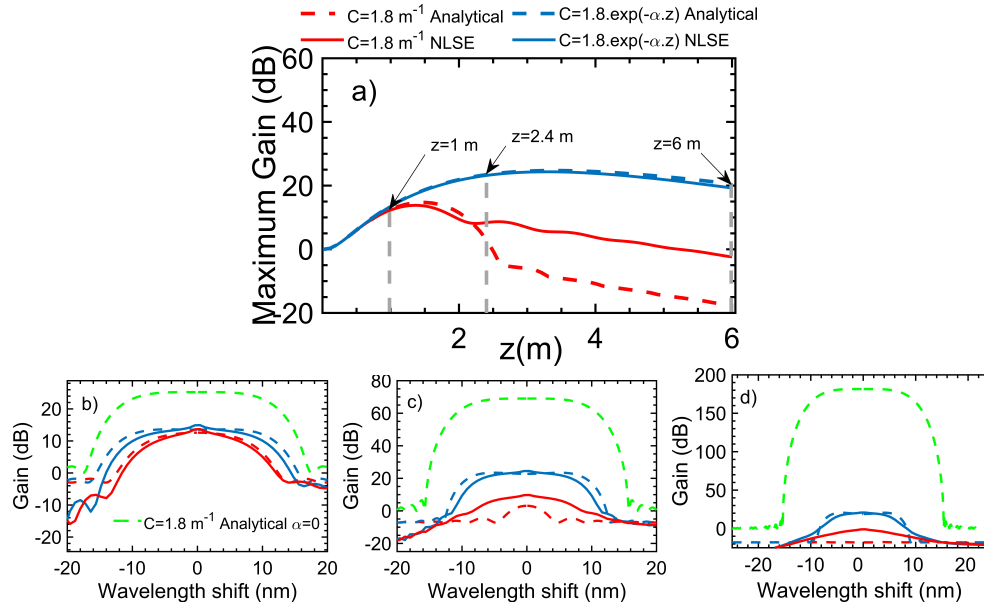
Fig. 2. Comparison of analytical predictions (dashed lines) with numerical results (solid lines) for $\beta_2 = -50 \ \text{ps}^2\text{km}^{-1}$: in panel a) we plot the maximum amplifier gain versus amplifier length for constant coupling (red lines) and spatially varying coupling (blue lines); in panel b) to d) we show a comparison of the gain spectrum obtained in theory and numerical simulations respectively for b) $z = 1$ m , c) $z = 2.4$ m and d) $z = 6$ m. As a reference panel b) to d) has 1 additional curve (green line) showing the spectrum, when there is no losses, i.e., $\alpha = 0$.

asymmetric gain spectrum in the spectral regions where gain is negligible or even negative. This is due to poor conversion efficiency in these spectral regions, and to the fact that the signal comb of CW waves was launched in the positive side of the spectrum, leading to very low power idlers being generated in the negative side of the spectrum. Thus, since gain was calculated as the output signal/idler power divided by input signal power, this generates an asymmetry in the gain spectrum. Additionally we have plotted, in green in Figs. 2(b)–2(d), the analytical curve for the gain spectrum for the case of constant coupling and $\alpha = 0$, in order to show that accounting for losses effect is strictly necessary to have realistic theoretical predictions of the amplifier behavior.

4. Single-waveguide vs. coupled dual-waveguide amplifier performances

We have compared through numerical simulations the performances of a coupled DWs amplifier with the ones of a SW amplifier (considering in DWs amplifier the pump power per waveguide the same as the pump power of the SW amplifier). Two different functional shapes of the spatially dependent coupling have been considered, namely $C(z) = C(0)e^{-c\alpha z}$ with $c = 2$ (red curve) and with $c = 1$ (black dashed curve). Regarding the SW amplifier we have considered both a constant and a spatially changing group velocity dispersion coefficient to make a fair comparison with results published in [31] regarding parametric amplification in tapered waveguides. In particular we chose $\beta_2(z) = \beta_2(0)e^{-\alpha z}$ (blue curve) and $\beta_2(z) = \beta_2(0) = -50 \ \text{ps}^2$/km (green curve). Figure 3(a) shows the maximum gain for all the 4 different amplifiers. Performances are very similar among the different scenarios, except for the constant dispersion SW amplifier which performs worse at large z. Blue and green curves are the cases reported in [31] and [30], respectively.

From Fig. 3(b) we can appreciate that distinct values of c, despite not affecting the maximum gain achieved, affect the maximum BW which was calculated by drawing a constant line, at the level of -3 dB below the maximum gain, and computing the intersection with the gain curve using [47]. Just the positive wavelength shift side of the gain spectrum is taken into account to calculate the BW. The discontinuity of red curve, observed at $z \approx 2.5$ m is related to the fact that for $z > 2.5$ m the flatness of the gain spectrum is lost and the spectral shape of the gain moves gradually from flat to something more related to the SW cases as can be seen in Fig. 3(d). Therefore the BW moves from being calculated as the difference, between an intersection point in the spectrum and the pump wavelength location, to be calculated as in the SW cases, where one will have 4 intersection points all likely to be different than the pump location. BW is larger for the red curve which leads to an higher BWG product given by $BWG(z) = 10 \log 10(G(z)) \cdot BW(z)$. BWG product is shown in Fig. 3(c). We note that the DW amplifier with spatially dependent coupling can perform, for particular amplifier lengths, up to almost twice as better than the SW amplifier both with and without dispersion management: the limitation imposed by the losses of the waveguide on the maximum attainable bandwidth and gain can be partially compensated by using two waveguides, with a longitudinal variation of the coupling coefficient. However SW amplifier outperforms the DW one, when $z \gtrsim 2$ m. Fig. 3(d) shows examples of the gain spectral shapes for $z = L$. Analogous curves to the ones presented in Fig. 3 are shown in Fig. 4, however this time considering $\beta_2 = -15$ ps^2/km; and similar conclusions to the ones made for larger anomalous dispersion can be drawn in this case too. We can observe that BW is much larger with smaller dispersion as it would be expected for a standard SW parametric amplifier.
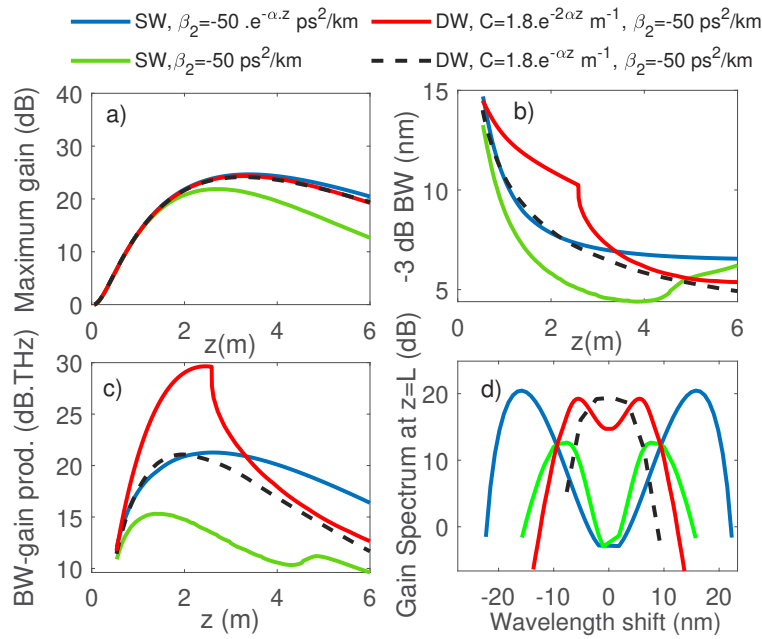

Fig. 3. SW vs. coupled DW amplifier performances in the form of a) peak gain b) bandwidth (BW) c) BWG product d) gain spectrum at $z = L$; when $\beta_2(0)$=-50 ps^2/km. Plots are from numerical solutions of the NLSEs.
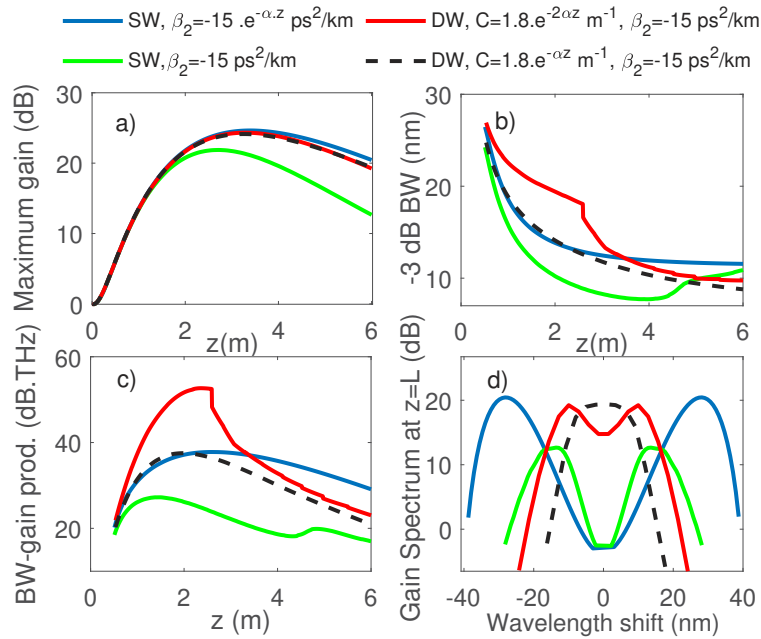
Fig. 4. SW vs. DW coupled waveguides amplifier performances in the form of a) peak gain b) bandwdith (BW) c) BWG product d) gain spectrum at $z = L$ when $\beta_2(0)$=-15 ps^2/km. Plots are from numerical solutions of the NLSEs.

5. Conclusions

In this work we have presented the analytical theory for an optical parametric amplifier consisting of two evanescently coupled lossy waveguides in presence of spatially dependent coupling. In the undepleted pump and weak sidebands approximation we have provided an approximated analytical solution for the signal and idler waves amplitudes evolution. We have shown that the analytical predictions agree well with numerical simulations in the variable coupling regime, while they exhibit some discrepancies at large propagation distances for constant coupling consistently with the existing theoretical models for standard lossy parametric amplifiers. Our model is suitable to the description of coupled silicon nitride waveguides and DWs silica fibers with coupled cores; and is especially relevant for waveguides where the effective length is smaller than, or comparable to, the nonlinear length. A comparison with single silicon nitride waveguide parametric amplifier, both with and without dispersion management, shows that the amplifier architecture studied in this paper can offer improved performances in terms of BW and BWG product too, thanks to the fact that spatially varying coupling can compensate for mismatch caused by dynamical pump attenuation. We envisage that advances in nonlinear waveguides fabrication techniques will make the architecture presented in this work appealing for real world applications of integrated optical parametric amplifiers. Furthermore alternative specific design of the spatially dependent coupling strength, and higher number of coupled optical modes, could be studied too hence enabling the possibility of engineering novel dissipative photonic devices based on nonlinear four-wave mixing.

Disclosures. The authors declare no conflicts of interest.

Data Availability. Data underlying the results presented in this paper are not publicly available at this time but may be obtained from the authors upon reasonable request.

References

1. R. J. Mears, L. Reekie, I. M. Jauncey, and D. N. Payne, "Low-noise erbium-doped fibre amplifier operating at 1.54μm," Electron. Lett. **23**(19), 1026–1028 (1987).
2. E. Desurvire, J. R. Simpson, and P. C. Becker, "High-gain erbium-doped traveling-wave fiber amplifier," Opt. Lett. **12**(11), 888–890 (1987).
3. M. Islam, "Raman amplifiers for telecommunications," IEEE J. Sel. Top. Quantum Electron. **8**(3), 548–559 (2002).
4. M. J. Conelly, *Semiconductor Optical Amplifiers* (Springer, 1st edn., 2002).
5. M. E. Mahric, *Fiber Optical Parametric Amplifiers, Oscillators and Related Devices: Theory, Applications, and Related Devices* (Cambridge University Press, 2007).
6. M. E. Marhic, P. A. Andrekson, P. Petropoulos, S. Radic, C. Peucheret, and M. Jazayerifar, "Fiber optical parametric amplifiers in optical communication systems," Laser Photonics Rev. **9**(1), 50–74 (2015).
7. J. Hansryd, P. A. Andrekson, M. Westlund, Jie Li, and P. Hedekvist, "Fiber-based optical parametric amplifiers and their applications," IEEE J. Sel. Top. Quantum Electron. **8**(3), 506–520 (2002).
8. S. Olsson, H. Eliasson, E. Astra, M. Karlsson, and P. A. Andrekson, "Long-haul optical transmission link using low-noise phase-sensitive amplifiers," Nat. Commun. **9**(1), 2513 (2018).
9. V. Gordienko, M. F. C. Stephens, A. E. El-Taher, and N. J. Doran, "Ultra-flat wideband single-pump raman-enhanced parametric amplification," Opt. Express **25**(5), 4810–4818 (2017).
10. V. Zakharov and L. Ostrovsky, "Modulation instability: the beginning," Phys. D (Amsterdam, Neth.) **238**(5), 540–548 (2009).
11. A. Hasegawa and W. Brinkman, "Tunable coherent ir and fir sources utilizing modulational instability," IEEE J. Quantum Electron. **16**(7), 694–697 (1980).
12. K. Tai, A. Hasegawa, and A. Tomita, "Observation of modulational instability in optical fibers," Phys. Rev. Lett. **56**(2), 135–138 (1986).
13. R. Stolen and J. Bjorkholm, "Parametric amplification and frequency conversion in optical fibers," IEEE J. Quantum Electron. **18**(7), 1062–1072 (1982).
14. Z. Tong, C. Lundström, P. A. Andrekson, C. J. McKinstrie, M. Karlsson, D. J. Blessing, E. Tipsuwannakul, B. J. Puttnam, H. Toda, and L. Gruner-Nielsen, "Towards ultrasensitive optical links enabled by low-noise phase-sensitive amplifiers," Nature **5**, 430–436 (2011).
15. Z. Tong, C. Lundström, P. A. Andrekson, M. Karlsson, and A. Bogris, "Ultralow noise, broadband phase-sensitive optical amplifiers, and their applications," IEEE J. Select. Topics Quantum Electron. **18**(2), 1016–1032 (2011).
16. H. Pakarzadeh and A. Zakery, "Modelling of noise suppression in gain-saturated fiber optical parametric amplifiers," Opt. Commun. **309**, 30–36 (2013).
17. P. A. Andrekson and M. Karlsson, "Fiber-based phase-sensitive optical amplifiers and their applications," Adv. Opt. Photonics **12**(2), 367–428 (2020).
18. M. F. C. Stephens, V. Gordienko, and N. J. Doran, "20 db net-gain polarization-insensitive fiber optical parametric amplifier with >2 THz bandwidth," Opt. Express **25**(9), 10597–10609 (2017).
19. J. Kim, O. Boyraz, J. Lim, and M. Islam, "Gain enhancement in cascaded fiber parametric amplifier with quasi-phase matching: theory and experiment," J. Lightwave Technol. **19**(2), 247–251 (2001).
20. S. Takasaka, Y. Mimura, M. Takahashi, R. Sugizaki, and H. Ogoshi, "Flat and broad amplification by quasi-phase-matched fiber optical parametric amplifier," *Optical Fiber Communication Conference*, (Optical Society of America, 2012), p. OTh1C.4.
21. V. Ribeiro, M. Karlsson, and P. Andrekson, "Parametric amplification with a dual-core fiber," Opt. Express **25**(6), 6234–6243 (2017).
22. V. Ribeiro, A. Lorences-Riesgo, P. Andrekson, and M. Karlsson, "Noise in phase-(in)sensitive dual-core fiber parametric amplification," Opt. Express **26**(4), 4050–4059 (2018).
23. M. Guasoni, F. Parmigiani, P. Horak, J. Fatome, and D. J. Richardson, "Intermodal four-wave mixing and parametric amplification in kilometer-long multimode fibers," J. Lightwave Technol. **35**(24), 5296–5305 (2017).
24. Z. Ye, P. Zhao, K. Twayana, M. Karlsson, P. A. Andrekson, and V. Torres-Company, "Ultralow-loss meter-long dispersion-engineered silicon nitride waveguides," *Conference on Lasers and Electro-Optics*, (Optical Society of America, 2021), p. SF1C.5.
25. N. M. Lüpken, T. Würthwein, K.-J. Boller, and C. Fallnich, "Optical parametric amplification in silicon nitride waveguides for coherent raman imaging," Opt. Express **29**(7), 10424–10433 (2021).
26. F. Gyger, J. Liu, F. Yang, J. He, A. S. Raja, R. N. Wang, S. A. Bhave, T. J. Kippenberg, and L. Thévenaz, "Observation of stimulated brillouin scattering in silicon nitride integrated waveguides," Phys. Rev. Lett. **124**(1), 013902 (2020).
27. Z. Ye, P. Zhao, K. Twayana, M. Karlsson, V. Torres-Company, and P. A. Andrekson, "Overcoming the quantum limit of optical amplification in monolithic waveguides," Sci. Adv. **7**(38), eabi8150 (2021).
28. M. Karlsson, "Modulational instability in lossy optical fibers," J. Opt. Soc. Am. B **12**(11), 2071–2077 (1995).
29. M. Alem, M. A. Soto, and L. Thévenaz, "Analytical model and experimental verification of the critical power for modulation instability in optical fibers," Opt. Express **23**(23), 29514–29532 (2015).

30. M. Karlsson, J. Schröder, P. Zhao, and P. A. Andrekson, "Analytic theory for parametric gain in lossy integrated waveguides," *Conference on Lasers and Electro-Optics*, (Optical Society of America, 2021), p. JTh3A.5.

31. P. Zhao, Z. Ye, K. Vijayan, C. Naveau, J. Schröder, M. Karlsson, and P. A. Andrekson, "Waveguide tapering for improved parametric amplification in integrated nonlinear Si$_3$N$_4$ waveguides," Opt. Express **28**(16), 23467–23477 (2020).

32. E. N. Tsoy, C. M. de Sterke, and F. K. Abdullaev, "Influence of two-photon absorption on modulational instability," J. Opt. Soc. Am. B **18**(8), 1144–1149 (2001).

33. S. Ramelow, A. Farsi, S. Clemmen, D. Orquiza, K. Luke, M. Lipson, and A. L. Gaeta, "Silicon-nitride platform for narrowband entangled photon generation," arXiv: Quantum Physics (2015).

34. A. D. Szabó, V. Ribeiro, C. B. Gaur, A. A. I. Ali, A. Mussot, Y. Quiquempois, G. Bouwmans, and N. J. Doran, "Dual-polarization c+l-band wavelength conversion in a twin-core highly nonlinear fibre," in *2021 Optical Fiber Communications Conference and Exhibition (OFC)*, (2021) pp. 1–3.

35. S. Trillo, S. Wabnitz, G. I. Stegeman, and E. M. Wright, "Parametric amplification and modulational instabilities in dispersive nonlinear directional couplers with relaxing nonlinearity," J. Opt. Soc. Am. B **6**(5), 889–900 (1989).

36. R. S. Tasgal and B. A. Malomed, "Modulational instabilities in the dual-core nonlinear optical fiber," Phys. Scr. **60**(5), 418–422 (1999).

37. R. Ganapathy, B. A. Malomed, and K. Porsezian, "Modulational instability and generation of pulse trains in asymmetric dual-core nonlinear optical fibers," Phys. Lett. A **354**(5-6), 366–372 (2006).

38. J. H. Li, K. S. Chiang, and K. W. Chow, "Modulation instabilities in two-core optical fibers," J. Opt. Soc. Am. B **28**(7), 1693–1701 (2011).

39. J. H. Li, K. S. Chiang, B. A. Malomed, and K. W. Chow, "Modulation instabilities in birefringent two-core optical fibres," J. Phys. B: At., Mol. Opt. Phys. **45**(16), 165404 (2012).

40. A. M. Rubenchik, E. V. Tkachenko, M. P. Fedoruk, and S. K. Turitsyn, "Power-controlled phase-matching and instability of cw propagation in multicore optical fibers with a central core," Opt. Lett. **38**(20), 4232–4235 (2013).

41. K. Nithyanandan, R. V. J. Raja, and K. Porsezian, "Modulational instability in a twin-core fiber with the effect of saturable nonlinear response and coupling coefficient dispersion," Phys. Rev. A **87**(4), 043805 (2013).

42. J. H. Li, K. S. Chiang, and C. R. Li, "Modulation instability in collinear three-core optical fibers," J. Opt. Soc. Am. B **34**(12), 2467–2477 (2017).

43. A. Govindarajan, B. A. Malomed, A. Mahalingam, and A. Uthayakumar, "Modulational instability in linearly coupled asymmetric dual-core fibers," Appl. Sci. **7**(7), 645 (2017).

44. S. Wu, W. Huang, P. Yang, S. Liu, and L. Chen, "Arbitrary phase-locking in mach–zehnder interferometer," Opt. Commun. **442**, 148–151 (2019).

45. R. Hui and M. O'Sullivan, "Basic instrumentation for optical measurement," Fiber Opt. Meas. Tech. **7**(2), 129–258 (2009).

46. B.-S. Kim, Y. Chung, and S.-H. Kim, "Split-step time-domain analysis of optical waveguide devices composed of a directional coupler and gratings," Opt. Lett. **25**(8), 530–532 (2000).

47. D. Schwarz, "Fast and robust curve intersections," MATLAB Central File Exchange (2022).